



Goethite Nanoparticle Aggregation: Effects of Buffers, Metal Ions, and 4-Chloronitrobenzene Reduction

Journal:	<i>Environmental Science: Nano</i>
Manuscript ID:	EN-ART-10-2013-000063.R1
Article Type:	Paper
Date Submitted by the Author:	06-Jun-2014
Complete List of Authors:	Stemig, Amanda; University of Minnesota - Twin Cities, Chemistry Yuwono, Virany; University of Minnesota - Twin Cities, Chemistry Arnold, William; University of Minnesota, Civil Engineering Penn, R.; University of Minnesota, Department of Chemistry

Impact statement for:

Goethite Nanoparticle Aggregation: Effects of Buffers, Metal Ions, and 4-Chloronitrobenzene Reduction

Amanda M. Stemig,^{a*} Virany M. Yuwono,^a William A. Arnold,^b and R. Lee Penn^a

Little is known about how natural and synthetic chemical species affect the reactivity of nanoparticles under environmentally relevant conditions. Specifically, aggregation state is predicted to strongly impact the accessible reactive surface area, and aggregation state is sensitive to solution conditions. It is essential to elucidate the links between reactivity and the aggregation states of nanoparticles. This work, which primarily focuses on the reductive degradation of 4-chloronitrobenzene by iron (II) adsorbed onto goethite surfaces, demonstrates that both the rates of degradation of environmental contaminants and the extent of nanoparticle aggregation are intimately linked. Changes to how reactors are prepared can dramatically affect the rates of reaction, the degree to which the goethite surfaces are charged, and the aggregation state of the iron oxide nanoparticles. Variables such as the buffer employed, as well as its concentration, as well as other additives, such as metal ions added, can result in substantial differences in experimental rate constants. This work combines quantification of degradation rates with quantification of aggregation state, including some analysis of direct images of aggregates in vitrified solution via cryogenic transmission electron microscopy.

Goethite Nanoparticle Aggregation: Effects of Buffers, Metal Ions, and 4-Chloronitrobenzene Reduction

Amanda M. Stemig,^a Virany M. Yuwono,^a William A. Arnold,^b and R. Lee Penn^a

Iron mineral systems are effective at transforming highly oxidized contaminants in natural and engineered systems. The rate at which the contaminant degrades may be influenced by the amount of available mineral surface area. This study used dynamic light scattering and cryogenic transmission electron microscopy to monitor changes in the aggregation state of goethite nanoparticles before and after reaction with 4-chloronitrobenzene (4-CINB). The effects of buffer identity, buffer concentration, and adsorbing metal identity on the goethite nanoparticle suspension characteristics and reactivity were monitored. Results demonstrate that buffers, which serve to hold pH nearly constant over the course of a reaction, are not benign additives in batch reactors. In fact, the identity and concentration of the buffer used strongly influences the rate of 4-CINB degradation by surface-associated ferrous ion. Increasing buffer concentration resulted in more compact goethite nanoparticle aggregates, and slower 4-CINB degradation was observed. In addition, the rate of degradation changed dramatically with changing buffer identity, with rates of reaction changing by an order of magnitude when switching from 4-(2-hydroxyethyl)-1-piperazineethanesulfonic acid (HEPES) to Tris(2-hydroxyethyl)amine (TEA). Finally, of the three metal ions selected (Ca(II), Fe(II), and Co(II)), the addition and adsorption of the two transition metals resulted in a dramatic decrease in the average nanoparticle aggregate size. Furthermore, oxidation of the adsorbed Fe(II), via O₂ or 4-CINB reduction, yielded decreases in zeta potential and increases in aggregate size. This work demonstrates that small changes in reaction parameters have a large effect on the rate of contaminant degradation through changes in nanoparticle aggregation state.

Introduction

Groundwater is an important fraction of the water supply throughout the United States. In 2005, 20% of water used in the United States was withdrawn from groundwater.¹ Many oxidized organic compounds, including chlorinated solvents, nitroaromatic compounds, and pesticides are present as contaminants in groundwater.^{2, 3} These chemicals have been designed with highly oxidized components in their structures, making them not only effective for their intended use but also stable in oxic environments. These compounds are frequently found as persistent contaminants in groundwater systems and, thus, pose an exposure risk to humans and wildlife.⁴⁻⁹ More than thirty years after the passage of the Comprehensive Environmental Response, Compensation, and Liability Act (i.e. Superfund), groundwater contamination still presents a challenge, in terms of remediation and the return of water resources to unrestricted use.¹⁰ While stability in oxic environments facilitates the transport of pollutants between soil and groundwater phases, the presence of oxidized functional groups suggests that reduction provides a means for the breakdown or remediation of these compounds.

In groundwater, a reductant known to reduce oxidized contaminants is Fe(II) associated with an iron mineral surface. Iron oxides such as ferrihydrite, goethite, magnetite, hematite, and lepidocrocite are ubiquitous in the environment and readily adsorb Fe(II) ions.¹¹ Degradation reactions of oxidized pollutants have been shown to be both efficient and rapid in these systems.¹²⁻¹⁹ This is due to the formation of reactive capacity after association of the Fe(II) ions with the iron mineral.^{20, 21} The amount of adsorbed Fe(II)^{13, 16, 22}, suspension pH^{13, 16, 23, 24}, and the adsorption of other constituents^{12, 18, 19, 22, 25-27} each affect the formation of reactive sites and dramatically alter the rate of contaminant reduction.

The number of reactive sites is directly related to specific surface area. Surface area increases with decreasing particle size, which means, on a mass normalized basis, the smallest mineral nanoparticles will contribute the most surface area.²⁸ Nanoparticles, however, are highly susceptible to aggregation, which can physically block access to reactive sites. This effect was shown by Vikesland *et al.*,²⁹ who demonstrated that by increasing the ionic strength of the suspension, magnetite nanoparticles aggregated, and the observed rate of carbon tetrachloride loss decreased.

The goal of this research is to elucidate the link between the aggregation state of iron oxide nanoparticles and their reactivity. Such nanoparticles may be present naturally¹¹ or introduced in an engineered remediation scheme.³⁰⁻³³ 4-Chloronitrobenzene (4-CINB) was selected as a model contaminant due to its previous use as a probe compound³⁴⁻³⁹ and its nitro group represents relevant classes of environmental contaminants (explosives and pesticides).⁴⁰

In addition to measuring kinetics of pollutant degradation, this study investigates changes in nanoparticle aggregation *in situ* by using dynamic light scattering (DLS) and cryogenic transmission electron microscopy (cryo-TEM). DLS measures the intensity of scattered light from suspended objects, enabling dynamic assessment of aggregation state. The working hypothesis is that larger aggregates will have more points of internal contact and thus, less surface area accessible to the surrounding solution for the degradation of environmental contaminants. An alternative hypothesis is that electron shuttling from one primary crystallite to another may result in faster kinetics than expected based on accessible surface area.^{41, 42} Cryo-TEM enables the

direct imaging of vitrified samples, which can be collected at any point during a reaction and thus serve as snapshots of the aggregation state during an experiment. Together, DLS and cryo-TEM enable quantitative characterization of aggregation state before, during, and after reaction.

Results and Discussion

Crucial to continued work in this area is consistency in experimental work so as to facilitate meaningful comparisons between laboratories. A survey of a sampling (78 in total) of recent research articles in the field (Figure 1)^{12-17, 19-26, 29, 34-36, 38, 39, 43-100} demonstrate substantial variation in the preparation of reactors for degradation reactions of environmental contaminants. Variations include buffer type, the order in which reagents (buffer, mineral, Fe(II), contaminant) are added, the number of equilibrations upon addition of reagents, the length of time allowed for equilibration, and number and identity of constituents present during each equilibration step. Buffer concentrations ranged from 0.4 to 100 mM, a mean of 32 mM, and median of 25 mM (with one extreme outlier of 1 M excluded from this analysis). Small differences in reaction conditions may be largely irrelevant or may fundamentally change the properties of the nanoparticle suspension such that comparisons of datasets become impossible. A goal of this work was to evaluate a subset of potentially important batch reactor variables so as to determine which variables of the experimental protocol do and do not facilitate quantitative and qualitative comparisons of reactivity in goethite nanoparticle systems.

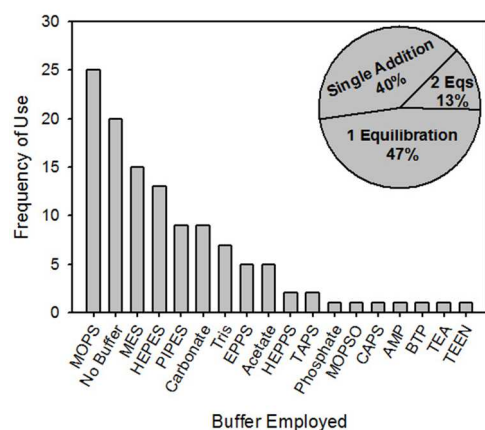


Figure 1: Graphical representation of iron mineral reactor preparation parameters from a sampling of 78 research articles. The buffer identity used in each study (note that the total exceeds 78 as multiple studies used various buffers) and the number of steps with equilibration periods in which the constituents are added (insert) were summarized to show the variation in procedures applied

Goethite particle characteristics

The goethite particles employed here had dimensions of 63.7 ± 22.9 nm by 8.9 ± 3.9 nm as measured by TEM and surface area of 136.8 m²/g as measured by N₂ adsorption. The mineral identity was confirmed by X-ray diffraction. Additional details are in the Supplementary Information (Figure S1, Table S1, and Figure S2).

Buffer concentration and metal ions: Pre-reaction

Aggregate sizes (from DLS) and zeta potentials (a surrogate for surface charge) in MOPS buffer before and after divalent metal ion addition are summarized in Table 1. In 20 mM MOPS buffer, the primary goethite particles form large aggregates. The value obtained using DLS, approximately 3000 nm, is near the upper limit for the DLS instrument, which means we can conclude only that the aggregates are large. However, the data point provides a basis for comparison to other conditions.

The concentration of buffer present within a reaction system affects aggregation of the goethite nanoparticles. The effect of buffer concentration was tested in the presence of 1 mM Fe(II) but prior to 4-CINB addition. MOPS buffer was selected for the

buffer concentration experiments due to its frequency of use in past studies (Figure 1).^{17, 26, 36} A general upward trend in aggregate size was observed via both DLS (Table 1) and cryo-TEM with increasing buffer concentration (Figure 2). For cryo-TEM analysis, goethite suspensions in 10, 20, and 50 mM were selected (6 images per concentration), and the images suggest that the average aggregate size is similar in 10 and 20 mM MOPS, but there is a significant size increase observed for goethite suspended in 50 mM MOPS. Despite the marked differences in size, the average aggregate density was statistically similar across all three buffer concentrations. Additional aggregate analysis revealed that a majority (>50%) of all nanoparticle contacts within an aggregate occurred along the major nanoparticle axis (Figure 2; complete TEM analysis results in SI, Figure S3). Previous results have demonstrated that the goethite {021} are the reactive surfaces, which could mean that such side-by-side contacts may not significantly affect accessible, reactive surface area.³⁴ Finally, zeta potential measurements clearly demonstrate a dramatic drop in surface charge as a function of increasing MOPS concentration. This parallels the increase in aggregate size as observed by DLS. With the observation that many of the particle-particle contacts occurs along the long-axis of the nanocrystals, one could hypothesize that MOPS molecules primarily adsorb onto the 110 type surfaces, resulting in a drop in surface charge for those surfaces. At pH 7, the particles are clearly positively charged, and the adsorption of deprotonated, negatively charged MOPS molecules results in a net drop in surface charge. If that drop in net charge primarily occurs via the 110 type surfaces, then aggregation across those surfaces may be promoted. Alternatively, MOPS may primarily adsorb onto the nanocrystal tips, resulting in steric repulsion between the tips, which could effectively promote aggregation in a side-by-side configuration.

Three M(II) ions were selected to determine their effect on goethite nanoparticle aggregate size and surface charge in 20 mM MOPS before the addition of 4-CINB (Table 1). Two goethite suspensions were prepared for each metal ion. Both Sample I and II were prepared in the same manner, except that the metal ion addition was delayed by 18 hours for Sample II. The hard metal ion, Ca(II), did not significantly alter either the aggregate diameter nor surface charge of nanoparticles. The small change observed in zeta potential is consistent with limited adsorption of Ca(II) onto the iron mineral surface. Upon addition of the transition metal ions Fe(II) and Co(II), however, nanoparticle aggregation dramatically decreased and zeta potential increased, which is consistent with adsorption of these cations onto the mineral surface, ultimately resulting in dispersal of the particles. Both trends hold for delayed addition of metal ions as demonstrated by the Sample II series. Overall, these results are consistent with expectations regarding the effect of surface charge on particle stability.

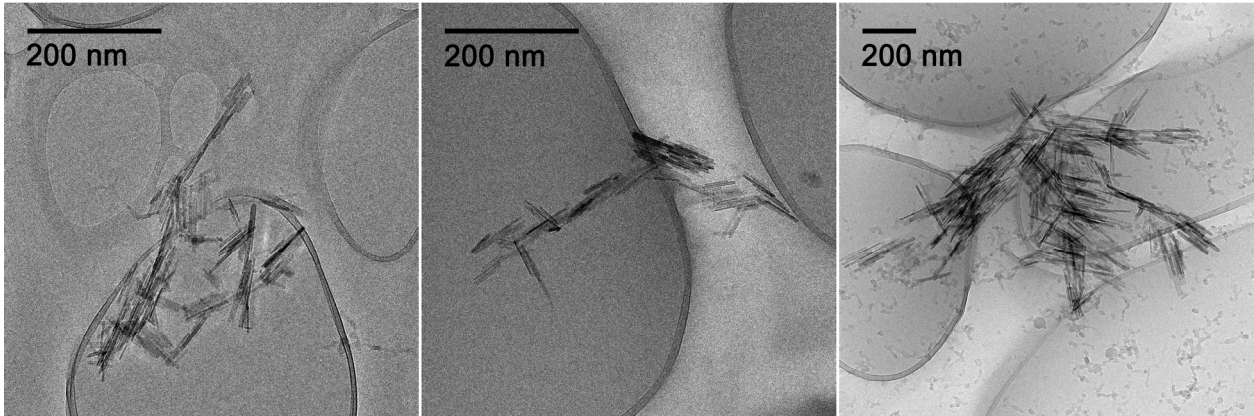
Figure 3 shows both the rate constant for 4-CINB degradation and the average pre-reaction aggregate size (determined by DLS and cryo-TEM) versus concentration of MOPS buffer. The maximum rate constant is observed for reactors containing 20 mM MOPS, and the rate constant decreases with further increases in buffer concentration. For MOPS concentrations less than 20 mM, the reaction rate decreased as the buffer concentration decreased. At 5 mM MOPS, the pH was less stable during the equilibration step and throughout the reaction, with the pH dropping by nearly one-third of a pH unit during equilibration and one-half a pH unit after reaction with 4CINB (Table S2). In contrast, at MOPS concentrations of 10 mM and higher, the pH dropped by one-tenth or less of a pH unit during the equilibration step. After reaction, the pH dropped by an additional tenth of a pH unit in the case of 10 mM MOPS reactor while the pH remained quite stable for MOPS concentrations of 20 mM and higher. The zeta potential measurements demonstrate a substantial difference between the 5, 10, and 20 mM MOPS reactors prior to addition of the 4-CINB, most notable is the difference between the 10 and 20 mM reactors. This will influence the kinetics because the sorption of Fe(II) is strongly pH dependent at circumneutral pHs and because the reduction of the aromatic nitro group is dependent on pH.^{37, 39, 101} Conversely, at buffer concentrations at and above 20 mM, the buffering capacity is sufficient to maintain a pH of 7 throughout the reaction. Thus, we conclude that the results demonstrating decreased reactivity with increasing aggregate size is consistent with a loss in accessible surface sites for 4-CINB degradation at the higher MOPS concentrations. In contrast, the lower MOPS concentrations do not provide adequate pH stability through the course of the reaction. Indeed, examination of the literature for results tracking ferrous ion adsorption to goethite, in combination with results from our laboratory using related conditions, demonstrates that the pH range of 6-7 is critical, with steep changes in ferrous ion adsorption as a function of modest changes in pH.^{75, 102-108}

Table 1. Goethite aggregate sizes and zeta potentials measured using dynamic light scattering

MOPS Concentration (mM)	Goethite only		Goethite + 1 mM Fe(II)		Goethite + 1 mM M(II)	
	Diameter (nm)	Zeta potential (mV)	Diameter (nm) ^a	Zeta potential (mV)	Diameter (nm) ^b	Zeta potential (mV) ^b
5			96 ± 4	46		
10			71 ± 4	42		
20	3055 ^d ± 1055 ^c	30.9 ± 2.4 ^c	260 ± 64	32	Fe(II): 240, 180	41, 38

					Co(II):180, 170 Ca ²⁺ : 2300, 1700	42, 41 22, 27
30			500 ± 150	17		
40			640 ± 130	15		
50			980 ± 540	9		

^aErrors represent standard deviation from three measurements on a single sample
^bFor each pair of numbers, the first a measurement taken when the metal was added after the goethite and MOPS buffer had equilibrated for 18 hours (Sample I) and the second is the measurement take when the metal was added after the goethite and MOPS buffer had equilibrated for 36 hours (Sample II)
^cAverage and standard deviation of nine separate preparations of goethite in 20 mM pH 7 MOPS
^dBeyond the upper quantitative detection limit of the instrumentation



[MOPS] (mM)	Average Length (nm)	Average Density (%)	Average Side to Side Contacts (%)
10	370 ± 110	37 ± 10	66
20	340 ± 71	35 ± 8	49
50	1100 ± 340	45 ± 5	55

Figure 2: Representative cryo-TEM images of goethite aggregates before the reaction in MOPS buffer at concentrations of 10 mM (A), 20 mM (B), and 50 mM (C). The table summarizes the size measurements, nanoparticle density calculations, and quantification of side to side nanoparticle contacts at each concentration (detailed image analysis results are included in Figure S3).

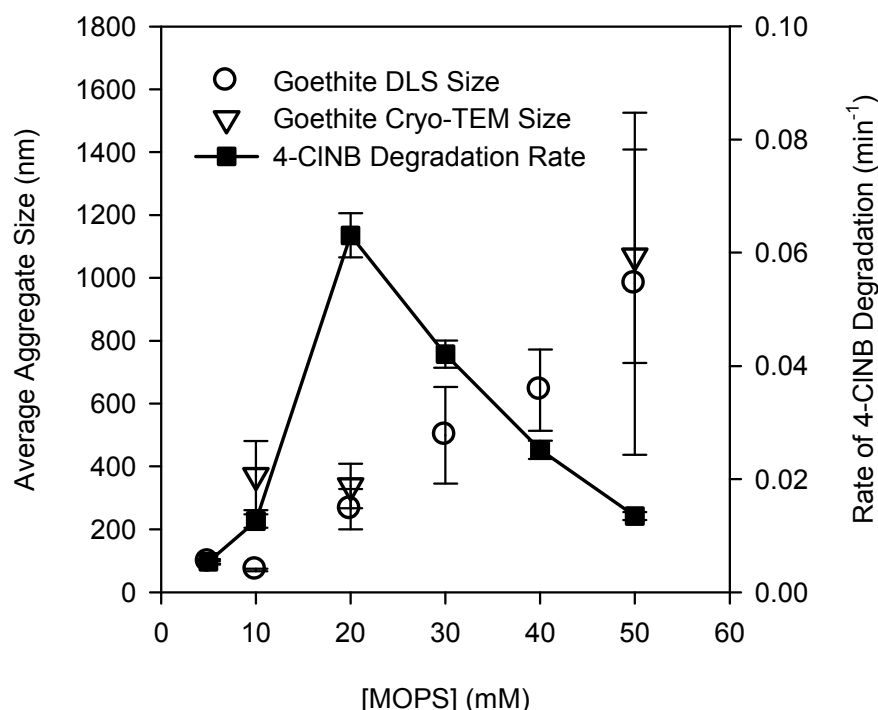


Figure 3: Average aggregate hydrodynamic diameter of goethite nanoparticles with 1.0 M Fe(II) before reaction as a function of MOPS concentration as determined by DLS and cryo-TEM measurements (left axis). Observed rate of 4-CINB degradation is plotted for each of the studied buffer concentrations and are connected by a line for ease of reading (right axis).

Buffer identity: Effect on aggregate size and reaction rates

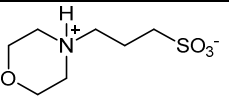
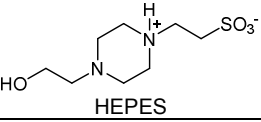
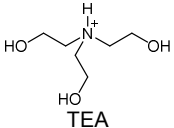
Buffers are commonly used to maintain a constant pH during a reaction, but their presence can result in substantial changes in aggregation state and surface chemistry,²⁵ as seen in Table 1 for MOPS. Goethite nanoparticles suspended in solutions containing 1 mM Fe(II) and HEPES buffer were the most dispersed before reaction with 4-CINB, and the aggregate sizes were 3-5 times larger for analogous suspensions prepared using MOPS and TEA buffers (Table 2). The zeta potentials, however, are similar for goethite particles in solutions prepared with the three buffers, indicating that the size differences are caused by a buffer-specific effect. In all cases, the introduction of 4-CINB leads to a dramatic increase in size, accompanied by a decrease in zeta potential, and aggregate sizes after reaction in HEPES buffer were 3-5 fold smaller than in MOPS or TEA (Figure 4; Table 2).

The observed differences in aggregate size may be explained by both the molecular and electronic nature of each buffer. At pH 7, the sulfate group on both MOPS and HEPES molecules is deprotonated, which allows for electrostatic interaction with the positively charged goethite surface. Because the zeta potential is similar for particles in all three buffers before the reaction, this suggests that pH and surface Fe(II), rather than buffer identity drives surface charge, and differences in aggregate size are intimately linked with the nature of the buffer molecules. If the sulfonate group is associated with the nanoparticle surface, the remainder of the molecule may act as a physical inhibitor to nanoparticle aggregation. The smaller nanoparticle aggregates suspended in HEPES buffer may be explained by steric hindrance because the HEPES molecules are larger. Another possibility is that the deprotonated amine group on the buffer sorbs to the surface, resulting in a net decrease in surface charge. The greater degree of aggregation in MOPS would then be due to greater adsorption, because more of the amine is deprotonated at pH 7 as compared to HEPES. (Attempts to quantify buffer sorption were unsuccessful). Unlike MOPS and HEPES, TEA molecules are predominantly positively charged at near-neutral pH and thus unlikely to be sorbed onto the positively charged goethite surface. As such, the nanoparticles are more likely to form larger aggregates in TEA than in solutions containing MOPS or HEPES.

While buffers such as MOPS, HEPES, and TEA enable adequate maintenance of pH, their presence is not passive with regard to mineral surface reactivity. The reduction of the nitro group to the amine requires the consumption of protons and the buffers provide a continuous source throughout the degradation process. The buffer identity, however, greatly affects the aggregation state of the goethite nanoparticles before the reaction with 4-CINB is initiated. Thus, trends can be compared, but quantitative comparisons remain challenging with different buffers and buffer concentration.

Results tracking the reduction rate of 4-CINB for reactors prepared with each of the three buffers are also reported in Table 2. The reaction is pseudo-first order in all buffers examined, and the rate in HEPES buffer solution is approximately 1.5 and 10 times faster than that in MOPS and TEA buffer solutions, respectively. This parallels the pre-reaction size trend. The largest aggregates (suspended in TEA) would be expected to have the smallest accessible surface area and the slowest rate of contaminant degradation, and the smallest aggregates (suspended in HEPES) would be expected to have the largest amount of accessible surface area and the fastest rate of degradation. Generally, the average hydrodynamic diameter increased dramatically upon injection of 4-CINB dissolved in methanol (Table 2; Figure 4). Greater size variation was observed when the nanoparticles were suspended in MOPS buffer (even considering that any value greater than 3000 nm is above the linear detection limit of the instrument). The variation in size is likely caused by turning the cuvettes over to re-suspend the settling particles. In the case of MOPS, the large variations may indicate breaking apart of loosely formed aggregates. Thus, the true size of the largest aggregates is difficult to quantify by DLS. It can be concluded, however, that the nanoparticle aggregates are dynamic throughout the degradation process and that the buffer greatly affects the average aggregate size and reactivity.

Table 2: Table displays the buffer molecular structure at pH 7 (and relevant pK_a), the average nanoparticle aggregate size before the addition of 4-CINB over the entire collection period (\pm SD), the average aggregate size over the 30 minutes after 4-CINB addition (\pm SD), and the observed rate of 4-CINB degradation (\pm 95% CI).

Buffer	pK_a	% in neutral amine form at pH 7	Pre-rxn size (nm)	Pre-rxn zeta potential (mV)	Post-4-CINB spike size (nm)	Post-4-CINB spike zeta potential (mV)	$k_{obs, 4-CINB}$ (min^{-1})
 MOPS	7.2	38.7	230 \pm 37	38	4300 ^a \pm 2200	33	0.056 \pm 0.001
 HEPES	7.6	20.1	72 \pm 2	41	770 \pm 340	38	0.091 \pm 0.005
 TEA	7.8	13.7	340 \pm 39	41	2400 \pm 720	34	0.009 \pm 0.001

^aBeyond the upper quantitative detection limit of the instrumentation

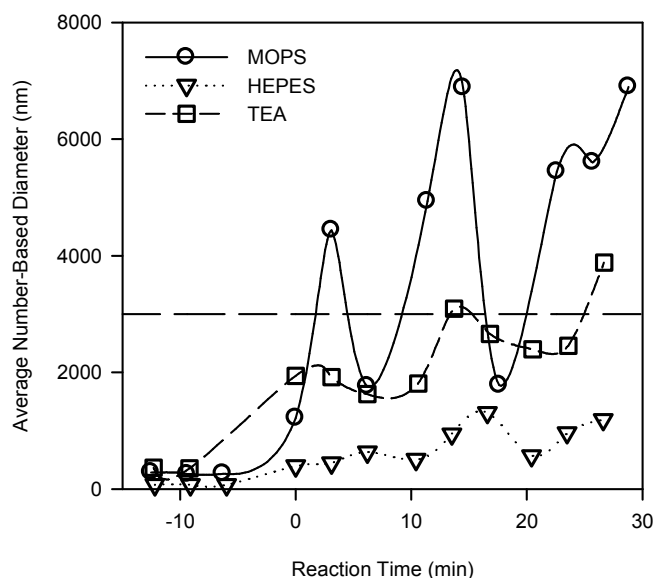


Figure 4: Observed changes in the average hydrodynamic aggregate diameter upon injection of methanolic 4-CINB into an Fe(II)-goethite suspension with 20 mM MOPS, HEPES, or TEA buffers as reported by DLS. Time zero represents 4-CINB injection time, thus pre-reaction samples are given a negative time value. The dashed line at 3000 nm represents the upper quantitative detection limit of the instrumentation.

Metal identity: Effect on aggregate size during reaction with 4-CINB and oxygen

4-CINB degradation was only observed in the Fe(II)-goethite system (Figure S4). Reaction in the presence of Ca(II) was neither expected nor observed (data not shown), because Ca(II) is redox inactive. Co(II) is redox active, but the reduction of the aromatic nitro group was essentially zero over the first 45 minutes (the time period over which substantial 4-CINB reduction occurred with Fe(II)) and significant loss of 4-CINB by HPLC analysis was not detected until ca. 24 hours.

Upon the addition of methanolic 4-CINB to goethite nanoparticle suspensions, the identity of the adsorbed metal ion impacted the aggregation state (Table 3). Goethite nanoparticles suspended with dissolved Co(II) remained well dispersed throughout the entire experiment (constant zeta potential), but no significant degradation of 4-CINB, despite the hypothesized redox activity of Co(II) in this system, was observed. In contrast, goethite nanoparticles suspended in a solution containing Fe(II) remained well dispersed until the addition of the methanolic 4-CINB, after which a substantial decrease in zeta potential and increase in aggregate size were observed as the 4-CINB reacted. The drop in zeta potential in the Fe(II)-goethite system (from 38 mV before introduction of 4-CINB to the system to 33 mV after) results from the oxidation of Fe(II) to Fe(III), and incorporation of the Fe(III) into the mineral phase as FeOOH thus reducing the surface charge. To see if the same effect would be observed with another oxidant, the systems were exposed to oxygen rather than 4-CINB. For Fe(II), exposure to oxygen also results in increasing aggregate size and decreased zeta potential (Table 3; Figure S5). Thus, oxidation of the Fe(II) clearly contributes to the observed increase in nanoparticle aggregate size. Co(II) is not oxidized under these conditions, and there are no changes to either the goethite aggregate size or surface charge.

Table 3: Effect of oxidant addition aggregate size and zeta potential for systems containing Fe(II) and Co(II)

Metal added	Pre-rxn size (nm)	Pre-rxn zeta potential (mV)	4-CINB		Oxygen	
			Post-rxn size (nm)	Post-rxn zeta potential	Post-rxn size (nm)	Post-rxn zeta potential

				(mV)		(mV)
Fe(II)	180	38	7930 ^a	33	1050 ^a , 6910 ^{b,d}	33 ^a , 23 ^b
Co(II)	170	41	840	39	130 ^c	40 ^c

^a Low oxygen exposure. The cap on the cell containing the suspension was opened for 15 seconds, re-closed, and the cell was gently turned over 7 times

^b High oxygen exposure. The cap was opened, reclosed, and the cell shaken. This procedure was repeated for 5 minutes.

^c A stream of oxygen was bubbled through the sample for 10 minutes.

^d Beyond the upper quantitative detection limit of the instrumentation

Experimental

Chemicals

All aqueous solutions were prepared with ultrapure water (18 MΩ·cm resistivity, Milli-Q, Millipore). NaHCO₃ (Sigma-Aldrich, 99.7-100.3%) and Fe(NO₃)₃·9 H₂O (Aldrich, 98+%) were used in the synthesis of goethite nanoparticles. 3-(N-morpholino)propanesulfonic acid (MOPS, Sigma-Aldrich, ≥99.5%), 4-(2-hydroxyethyl)-1-piperazineethanesulfonic acid (HEPES, Sigma-Aldrich), and Tris(2-hydroxyethyl)amine (TEA, Baker Analyzed Reagent, >99.0%) were adjusted to pH 7 with HCl (BDH Aristar) or NaOH (Mallinkrodt Chemicals, 99%), vacuum filtered, and deoxygenated by nitrogen sparging (Matheson, grade 99.9998%). 4-chloronitrobenzene (4CINB, 99%) was obtained from Acros Organics. Acetonitrile (HPLC grade) and ammonium acetate (Fluka Analytical, HPLC, ≥99.0%) were used in high pressure liquid chromatography (HPLC) analysis. FeCl₂·4H₂O (Fisher Scientific, 101.0%), CoCl₂ (Mallinkrodt Chemicals, 98.8%), and CaCl₂ (Fisher Scientific, 99%) were used to prepare metal ion solutions.

Goethite Nanoparticle Synthesis

Goethite nanorods were synthesized by Chun et al.³⁴ Particle size distribution and X-ray diffraction pattern of the synthesized particles are provided in the Supplementary Information.

4-CINB Degradation Reactions

Experiments were carried out in 50 mL serum bottles and were prepared in an anaerobic chamber (Coy Laboratory Products, 5% H₂/95% N₂) and sealed with a PTFE-lined aluminum crimp cap. Reactors contained approximately 0.325 g/L goethite nanoparticles and deoxygenated pH 7 MOPS, HEPES, or TEA buffer. The reactor was removed from the anaerobic chamber, sonicated on ice for two hours (AquaSonic 150HT, VWR Scientific), and returned to the anaerobic chamber. The solutions of 1.0 M CoCl₂, CaCl₂, and acidified FeCl₂ were prepared in the glove bag and added to the serum bottle to yield a final concentration of 1.0 mM of the desired cation. The suspension was stirred along the longitudinal axis of the serum bottle on a magnetic stir plate (IKAMAG RO10power, IKA Works Inc.) and allowed to equilibrate for approximately 18 hours. The serum bottle was wrapped in aluminum foil to prevent degradation by photolysis. To initiate an experiment, either a deoxygenated methanolic or MOPS solution of 4-CINB was added to the reactor to yield an initial concentration of 100 μM.

At desired reaction times, 0.5 mL samples of the suspension were filtered with a 0.2 μm nylon membrane. The concentration of 4-CINB was quantified by an Agilent 1100 Series system equipped with an ultraviolet detector. A 20 μL sample was injected onto a Zorbax SB-C18 column (4.6 mm × 150 mm, 5 μm). The 70:30 acetonitrile:ammonium acetate (10% v/v acetonitrile/ammonium acetate 1g/L, pH 7) mobile phase was operated at a flow rate of 0.7 mL/min for a total separation time of 7 minutes. The absorbance at 254 nm was monitored. The retention time of 4-CINB was 4.42 minutes, and 4-chloroaniline (the ultimate degradation product of the reduction) eluted at 3.22 minutes.

Nanoparticle Characterization

XRD

Nanoparticle composition was analyzed by XRD using a PANalytical X-Pert PRO MPD X-ray diffractometer equipped with a cobalt source, iron filter, and an X-Celerator detector over the range 20-105 °2θ at a scan rate of 0.0235 ° per second with an effective 90 seconds per step. The resulting patterns were compared to the reference powder diffraction files (PDFs) of ferrihydrite (#29-0712), magnetite (#19-0629), and goethite (#29-0713).

Zeta Potential

A 2.5 mL sample of prepared goethite suspension was removed the anaerobic chamber and placed in a Brookhaven Instruments Corporation ZetaPALS Zeta Potential Analyzer 90Plus/BI-MAS Multi Angle Particle Sizing Option DLS instrument where the zeta potential was measured. Data collection parameters consisted of: 5 runs of 20 cycles each, estimated sample size of 3000 nm, sample concentration of 0.32 mg/mL, 25°C, aqueous suspension, pH 7, and Smoluchowski zeta potential model.

DLS

A 2.5 mL sample of goethite suspension was transferred to an air-tight quartz cuvette inside the anaerobic chamber from a prepared reactor prior to 4-CINB introduction. The sample was removed from the chamber and placed into the DLS instrument

where the hydrodynamic diameter was continuously measured for approximately 30 minutes. To make measurements during reaction, the 4-CINB solution was injected into the cuvette and the hydrodynamic diameter was measured for an additional 30 to 60 minutes. Run parameters consisted of triplicate measurements of a sequence of 9 runs (20 second run duration, total analysis time of 9 minutes), a dust filter value of 500, the assumption that the particles are thin shells (refractive index values of 1.590 and 0.000 for the real and imaginary components, respectively), sample temperature of 25 °C, laser wavelength of 657 nm, and a detection angle of 90°. Every 9 minutes, the cuvette was taken out of the instrument and gently inverted twice to prevent particle sedimentation. The hydrodynamic diameters reported are the number-based mean diameter of the aggregates. Reported pre-reaction sizes are the average and standard deviation over the first 30 minutes while the post-reaction sizes are the final average hydrodynamic diameter recorded after 4-CINB addition.

Cryo-TEM

Approximately 3 µL of goethite nanoparticles suspended in MOPS buffer was applied to a 3 mm 200-mesh lacey carbon coated copper grid (SPI Supplies). The grid was blotted with filter paper in a 100% humidity environment for 2 seconds to create a thin film of suspension inside a controlled humidified chamber (Vitrobot Mark IV, FEI Company). The grid was plunged into a well of liquid ethane and transferred under liquid nitrogen to a cryo-TEM holder and analyzed by a FEI Technai F30 TEM. Images were analyzed using ImageJ 1.44p equipped with additional plugins from the MBF ImageJ for Microscopy Collection. Angles between adjacent particles were measured and counted for each aggregate to determine the frequency of side-to-side contacts. The particle density was determined by enclosing the aggregate in a polygon in which all corners pointed out, converting the image to black (background) and white (nanoparticles), and counting the number particle pixels in relation to the number of total polygon pixels. Results for each concentration are reported as the average of six representative images.

Conclusions

The size of goethite nanoparticle aggregates is dramatically reduced by adsorption of a transition metal ion, which imparts a positive charge to the surface. Only Fe(II) was found to promote the degradation of 4-CINB, and oxidation of the added Fe(II) by 4-CINB or oxygen resulted in increased aggregation. The different oxidants (atmospheric oxygen, pure oxygen, or 4-CINB reduction) all led to increases in aggregation state. Thus, it appears that the oxidant identity is not a factor in aggregate size increase, but rather the fact that oxidation occurs.

Results also demonstrate aggregation state of goethite nanoparticles is affected by the chemical conditions in the reactor which in turn affects reactivity with contaminants. The buffer selected to maintain reactor pH and the buffer concentration used both alter the average nanoparticle size and, by extension, the surface area available for 4-CINB degradation. Both the electronic and structural nature of the buffer molecule can explain the observed trends of both the goethite aggregate size and observed rates of 4-CINB degradation. Zwitterionic buffers with spatial charge separation are better at preventing nanoparticle aggregation and yield faster rates of degradation than buffers with only a central positive charge.

In addition, the concentration of the buffer played a role in both the aggregation state and, to a greater extent, the rate of 4-CINB degradation. At high buffer concentrations, the aggregates were larger and more densely packed on average (due to buffer association with the surface as evidenced by changes in zeta potential than those suspended in lower buffer concentrations. This increase in packing is the hypothesized source of the decreased rate of 4-CINB degradation. If the buffer concentration was not sufficient to maintain a stable pH, effects on the extent of Fe(II) sorption, and thus reactivity of the nanoparticles were observed. These dramatic effects of buffer identity and concentration on aggregation state and degradation rate calls into question the appropriateness of using biological buffers within batch reactors to simulate the reactivity of nanoparticles in natural aquatic systems. It appears that if it is desired to it will be necessary to use carbonate buffer to understand how nanoparticles react and aggregate in the environment.

Acknowledgements

Tram Anh Do is acknowledged for the collection of experimental data and other substantial contributions to this work. The authors would like to thank the University of Minnesota and the National Science Foundation (NSF-1012193) for financial support. Parts of this work were carried out in the Characterization Facility, University of Minnesota, a member of the NSF-funded Materials Research Facilities Network (www.mrfln.org) via the MRSEC program.

Notes and references

^a Department of Chemistry, 207 Pleasant St SE, Minneapolis, MN, 55455, USA. Fax: 01 612-626-7541; Tel: 01 612-624-6000; E-mail: rleppenn@umn.edu

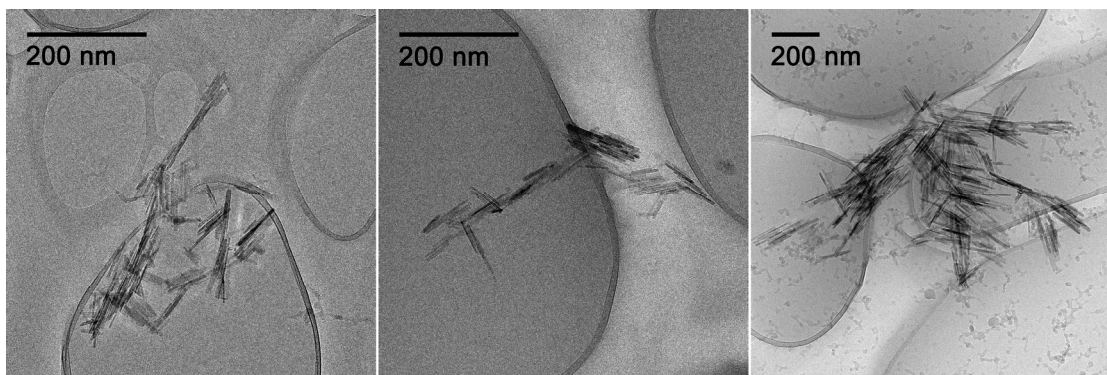
^b Department of Civil Engineering, 500 Pillsbury Dr SE, Minneapolis, MN, 55455, USA. Fax: 01 612-626-7750; Tel: 01 612-625-8582; E-mail: arnold032@umn.edu

† Electronic Supplementary Information (ESI) available: [details of any supplementary information available should be included here]. See DOI: 10.1039/b000000x/

1. N. J. Barber, *U.S. Geological Survey Fact Sheet 2009-3098*, 2009, 2 p.
2. C. A. Eddy-Miller, T. T. Bartos and M. L. Taylor, *U.S. Geological Survey Scientific Investigations Report*, 2013, 45 p.
3. K. L. Smalling, J. L. Orlando, D. Calhoun, W. A. Battaglin and K. M. Kuivila, *U.S. Geological Survey Data Series 707*, 2012, 40 p.
4. P. J. Squillace, J. C. Scott, M. J. Moran, B. T. Nolan and D. W. Kolpin, *Environ. Sci. Technol.*, 2002, **36**, 1923-1930.
5. R. J. Gilliom, *Environ. Sci. Technol.*, 2007, **41**, 3408-3414.
6. D. W. Kolpin, J. E. Barbash and R. J. Gilliom, *Environ. Sci. Technol.*, 1998, **32**, 558-566.
7. J. D. Fallon, *Geological Survey Fact Sheet 066-00*, 2000, 4 p.
8. K. L. Smalling, G. M. Fellers, P. M. Kleeman and K. M. Kuivila, *Environ. Toxicol. Chem.*, 2013, **32**, 2026-2034.
9. R. W. Gale, M. J. Tanner, M. S. Love, M. M. Nishimoto and D. M. Schroeder, *U.S. Geological Survey Open-File Report 2013-1046*, 2013, 31 p. and supplemental tables.
10. *Alternatives for Managing the Nation's Complex Contaminated Groundwater Sites*, The National Academies Press, 2013.
11. R. M. Cornell and U. Schwertmann, *The Iron Oxides: Structure, Properties, Reactions, Occurrences and Uses*, 2nd edn., Wiley-VCH, 2003.
12. R. A. Maithreepala and R.-a. Doong, *Environ. Sci. Technol.*, 2004, **38**, 6676-6684.
13. K. Pecher, S. B. Haderlein and R. P. Schwarzenbach, *Environ. Sci. Technol.*, 2002, **36**, 1734-1741.
14. M. Elsner, S. B. Haderlein, T. Kellerhals, S. Luzi, L. Zwank, W. Angst and R. P. Schwarzenbach, *Environ. Sci. Technol.*, 2004, **38**, 2058-2066.
15. C. L. Chun, R. M. Hozalski and W. A. Arnold, *Environ. Sci. Technol.*, 2005, **39**, 8525-8532.
16. J. E. Amonette, D. J. Workman, D. W. Kennedy, J. S. Fruchter and Y. A. Gorby, *Environ. Sci. Technol.*, 2000, **34**, 4606-4613.
17. T. P. Klupinski, Y.-P. Chin and S. J. Traina, *Environ. Sci. Technol.*, 2004, **38**, 4353-4360.
18. E. J. O'Loughlin, K. M. Kemner and D. R. Burris, *Environ. Sci. Technol.*, 2003, **37**, 2905-2912.
19. R. A. Maithreepala and R.-a. Doong, *Environ. Sci. Technol.*, 2004, **38**, 260-268.
20. M. Elsner, R. P. Schwarzenbach and S. B. Haderlein, *Environ. Sci. Technol.*, 2004, **38**, 799-807.
21. A. G. B. Williams and M. M. Scherer, *Environ. Sci. Technol.*, 2004, **38**, 4782-4790.
22. D. Colón, E. J. Weber and J. L. Anderson, *Environ. Sci. Technol.*, 2008, **42**, 6538-6543.
23. K. M. Danielsen and K. F. Hayes, *Environ. Sci. Technol.*, 2004, **38**, 4745-4752.
24. T. P. Klupinski and Y.-P. Chin, *Environ. Sci. Technol.*, 2003, **37**, 1311-1318.
25. A. Buchholz, C. Laskov and S. B. Haderlein, *Environ. Sci. Technol.*, 2011, **45**, 3355-3360.
26. J. A. Hakala, Y.-P. Chin and E. J. Weber, *Environ. Sci. Technol.*, 2007, **41**, 7337-7342.
27. J. A. Hakala and Y.-P. Chin, *J. Agric. Food Chem.*, 2010, **58**, 12840-12846.
28. J. J. Erbs, B. Gilbert and R. L. Penn, *J. Phys. Chem. C*, 2008, **112**, 12127-12133.
29. P. J. Vikesland, A. M. Heathcock, R. L. Rebodos and K. E. Makus, *Environ. Sci. Technol.*, 2007, **41**, 5277-5283.
30. J. Narr, T. Viraraghavan and Y.-C. Jin, *Fresenius Environ. Bull.*, 2007, **16**, 320-329.
31. D. H. Phillips, T. V. Nooten, L. Bastiaens, M. I. Russell, K. Dickson, S. Plant, J. M. E. Ahad, T. Newton, T. Elliot and R. M. Kalin, *Environ. Sci. Technol.*, 2010, **44**, 3861-3869.
32. N. Savage and M. S. Diallo, *J. Nanopart. Res.*, 2005, **7**, 331-342.
33. J. Theron, J. A. Walker and T. E. Cloete, *Crit. Rev. Microbiol.*, 2008, **34**, 43-69.
34. C. L. Chun, R. L. Penn and W. A. Arnold, *Environ. Sci. Technol.*, 2006, **40**, 3299-3304.
35. A. Hartenbach, T. B. Hofstetter, M. Berg, J. Bolotin and R. P. Schwarzenbach, *Environ. Sci. Technol.*, 2006, **40**, 7710-7716.
36. J. Klausen, S. P. Tröber, S. B. Haderlein and R. P. Schwarzenbach, *Environ. Sci. Technol.*, 1995, **29**, 2396-2404.
37. D. Naka, D. Kim and T. J. Strathmann, *Environ. Sci. Technol.*, 2006, **40**, 3006-3012.
38. A. Neumann, T. B. Hofstetter, M. Lüssi, O. A. Cirpka, S. Petit and R. P. Schwarzenbach, *Environ. Sci. Technol.*, 2008, **42**, 8381-8387.
39. C. A. Schultz and T. J. Grundl, *Environ. Sci. Technol.*, 2000, **34**, 3641-3648.
40. R. P. Schwarzenbach, P. M. Gschwend and D. M. Imboden, *Environmental Organic Chemistry*, Second edn., John Wiley & Sons, Inc., Hoboken, NJ, 2003.
41. M. M. Scherer, B. A. Balko and P. G. Tratnyek, *Mineral-Water Interfacial Reactions*, January 15, 1999, 301-322.
42. K. M. Rosso, S. V. Yanina, C. A. Gorski, P. Larese-Casanova and M. M. Scherer, *Environ. Sci. Technol.*, 2010, **44**, 61-67.
43. C. Gu, H. Jia, H. Li, B. J. Teppen and S. A. Boyd, *Environ. Sci. Technol.*, 2010, **44**, 4258-4263.
44. S.-H. Kang and W. Choi, *Environ. Sci. Technol.*, 2008, **43**, 878-883.
45. Y.-S. Keum and Q. X. Li, *Chemosphere*, 2004, **54**, 255-263.
46. W. Lee and B. Batchelor, *Environ. Sci. Technol.*, 2002, **36**, 5147-5154.

47. L. Yan and G. W. Bailey, *J. Colloid Interface Sci.*, 2001, **241**, 142-153.
48. A. Agrawal and P. G. Tratnyek, *Environ. Sci. Technol.*, 1995, **30**, 153-160.
49. L. Wu, B. L. Beard, E. E. Roden, C. B. Kennedy and C. M. Johnson, *Geochim. Cosmochim. Acta*, 2010, **74**, 4249-4265.
50. Y. T. He, J. T. Wilson and R. T. Wilkin, *Geochim. Cosmochim. Acta*, 2010, **74**, 2025-2039.
51. K. Amstatter, T. Borch, P. Larese-Casanova and A. Kappler, *Environ. Sci. Technol.*, 2010, **44**, 102-108.
52. X. Liang, R. P. Philp and E. C. Butler, *Chemosphere*, 2009, **75**, 63-69.
53. H.-S. Kim, W.-H. Kang, M. Kim, J.-Y. Park and I. Hwang, *Chemosphere*, 2008, **73**, 813-819.
54. P. Larese-Casanova and M. M. Scherer, *Environ. Sci. Technol.*, 2008, **42**, 3975-3981.
55. T. Peretyazhko, J. M. Zachara, S. M. Heald, B.-H. Jeon, R. K. Kukkadapu, C. Liu, D. Moore and C. T. Resch, *Geochim. Cosmochim. Acta*, 2008, **72**, 1521-1539.
56. D. M. Cwiertny, R. M. Handler, M. V. Schaefer, V. H. Grassian and M. M. Scherer, *Geochim. Cosmochim. Acta*, 2008, **72**, 1365-1380.
57. C. L. Chun, R. M. Hozalski and W. A. Arnold, *Environ. Sci. Technol.*, 2007, **41**, 1615-1621.
58. J.-Y. Lee, R. M. Hozalski and W. A. Arnold, *Chemosphere*, 2007, **66**, 2127-2135.
59. D. Colón, E. J. Weber, J. L. Anderson, P. Winget and L. A. Suarez, *Environ. Sci. Technol.*, 2006, **40**, 4449-4454.
60. E. Silvester, L. Charlet, C. Tournassat, A. Géhin, J.-M. Grenèche and E. Liger, *Geochim. Cosmochim. Acta*, 2005, **69**, 4801-4815.
61. H. D. Pedersen, D. Postma, R. Jakobsen and O. Larsen, *Geochim. Cosmochim. Acta*, 2005, **69**, 3967-3977.
62. R. A. Maithreepala and R.-a. Doong, *Environ. Sci. Technol.*, 2005, **39**, 4082-4090.
63. E. C. Butler, Y. Dong, L. R. Krumholz, X. Liang, H. Shao and Y. Tan, *Aquatic Redox Chemistry*, **January 1, 2011**, 519-538.
64. P. Larese-Casanova, D. M. Cwiertny and M. M. Scherer, *Environ. Sci. Technol.*, 2010, **44**, 3765-3771.
65. R. S. Cutting, V. S. Coker, N. D. Telling, R. L. Kimber, C. I. Pearce, B. L. Ellis, R. S. Lawson, G. van der Laan, R. A. D. Patrick, D. J. Vaughan, E. Arenholz and J. R. Lloyd, *Environ. Sci. Technol.*, 2010, **44**, 2577-2584.
66. C. A. Gorski, J. T. Nurmi, P. G. Tratnyek, T. B. Hofstetter and M. M. Scherer, *Environ. Sci. Technol.*, 2010, **44**, 55-60.
67. F.-b. Li, L. Tao, C.-h. Feng, X.-z. Li and K.-w. Sun, *Environ. Sci. Technol.*, 2009, **43**, 3656-3661.
68. C. A. Gorski and M. M. Scherer, *Environ. Sci. Technol.*, 2009, **43**, 3675-3680.
69. N. B. Tobler, T. B. Hofstetter, K. L. Straub, D. Fontana and R. P. Schwarzenbach, *Environ. Sci. Technol.*, 2007, **41**, 7765-7772.
70. N. B. Tobler, T. B. Hofstetter and R. P. Schwarzenbach, *Environ. Sci. Technol.*, 2007, **41**, 7773-7780.
71. P. Larese-Casanova and M. M. Scherer, *Environ. Sci. Technol.*, 2007, **41**, 471-477.
72. L. Zwank, M. Elsner, A. Aeberhard, R. P. Schwarzenbach and S. B. Haderlein, *Environ. Sci. Technol.*, 2005, **39**, 5634-5641.
73. S.-Y. Oh, D. K. Cha, B. J. Kim and P. C. Chiu, *Environ. Sci. Technol.*, 2004, **38**, 3723-3730.
74. K. B. Gregory, P. Larese-Casanova, G. F. Parkin and M. M. Scherer, *Environ. Sci. Technol.*, 2004, **38**, 1408-1414.
75. B.-H. Jeon, B. A. Dempsey and W. D. Burgos, *Environ. Sci. Technol.*, 2003, **37**, 3309-3315.
76. P. J. Vikesland and R. L. Valentine, *Environ. Sci. Technol.*, 2002, **36**, 512-519.
77. L. A. Totten, U. Jans and A. L. Roberts, *Environ. Sci. Technol.*, 2001, **35**, 2268-2274.
78. M. S. Elovitz and E. J. Weber, *Environ. Sci. Technol.*, 1999, **33**, 2617-2625.
79. E. C. Butler and K. F. Hayes, *Environ. Sci. Technol.*, 1998, **32**, 1276-1284.
80. J. Klausen, S. B. Haderlein and R. P. Schwarzenbach, *Environ. Sci. Technol.*, 1997, **31**, 2642-2649.
81. B. A. Holmén, M. I. Tejedor-Tejedor and W. H. Casey, *Langmuir*, 1997, **13**, 2197-2206.
82. M. Tong, S. Yuan, H. Long, M. Zheng, L. Wang and J. Chen, *J. Contam. Hydrol.*, 2011, **122**, 16-25.
83. Y. Xie and D. M. Cwiertny, *Environ. Sci. Technol.*, 2010, **44**, 8649-8655.
84. L. Tao, F. Li, Y. Wang and K. Sun, *Clays Clay Miner.*, 2010, **58**, 682-690.
85. A. G. B. Williams, K. B. Gregory, G. F. Parkin and M. M. Scherer, *Environ. Sci. Technol.*, 2005, **39**, 5183-5189.
86. S. Chakraborty, F. Favre, D. Banerjee, A. C. Scheinost, M. Mullet, J.-J. Ehrhardt, J. Brendle, L. Vidal and L. Charlet, *Environ. Sci. Technol.*, 2010, **44**, 3779-3785.
87. A. Neumann, T. B. Hofstetter, M. Skarpeli-Liati and R. P. Schwarzenbach, *Environ. Sci. Technol.*, 2009, **43**, 4082-4089.
88. F. Monteil-Rivera, L. Paquet, A. Halasz, M. T. Montgomery and J. Hawari, *Environ. Sci. Technol.*, 2005, **39**, 9725-9731.
89. Y.-H. Tee, L. Bachas and D. Bhattacharyya, *J. Phys. Chem. C*, 2009, **113**, 9454-9464.
90. C. L. Chun, D. R. Baer, D. W. Matson, J. E. Amonette and R. L. Penn, *Environ. Sci. Technol.*, 2010, **44**, 5079-5085.
91. J. T. Nurmi, P. G. Tratnyek, V. Sarathy, D. R. Baer, J. E. Amonette, K. Pecher, C. Wang, J. C. Linehan, D. W. Matson, R. L. Penn and M. D. Driessen, *Environ. Sci. Technol.*, 2005, **39**, 1221-1230.
92. K. M. Danielsen, J. L. Gland and K. F. Hayes, *Environ. Sci. Technol.*, 2005, **39**, 756-763.
93. R. B. Merola, E. D. Fournier and M. M. McGuire, *Langmuir*, 2007, **23**, 1223-1226.
94. R. J. Hanoch, H. Shao and E. C. Butler, *Chemosphere*, 2006, **63**, 323-334.
95. S. Dixit and J. G. Hering, *Chem. Geol.*, 2006, **228**, 6-15.
96. Q. Wang, N. Cissoko, M. Zhou and X. Xu, *Phys. Chem. Earth*, 2011, **36**, 442-446.

97. R. Welch and R. G. Riefler, *Environ. Eng. Sci.*, 2008, **25**, 1255-1262.
98. G. V. Nano and T. J. Strathmann, *J. Colloid Interface Sci.*, 2008, **321**, 350-359.
99. S.-Y. Oh, D. K. Cha, B. J. Kim and P. C. Chiu, *Environ. Sci. Technol.*, 2005, **24**, 2812-2819.
100. W. Lee and B. Batchelor, *Environ. Sci. Technol.*, 2002, **36**, 5348-5354.
101. P. G. Tratnyek and D. L. Macalady, *J. Agric. Food Chem.*, 1989, **37**, 248-254.
102. E. Liger, L. Charlet and P. Van Cappellen, *Geochim. Cosmochim. Acta*, 1999, **63**, 2939-2955.
103. L. Charlet, E. Liger and P. Gerasimo, *J. Environ. Eng.*, 1998, **124**, 25-30.
104. L. Charlet, E. Silvester and E. Liger, *Chem. Geol.*, 1998, **151**, 85-93.
105. J. M. Zachara, S. C. Smith and J. K. Fredrickson, *Geochim. Cosmochim. Acta*, 2000, **64**, 1345-1362.
106. B. R. Coughlin and A. T. Stone, *Environ. Sci. Technol.*, 1995, **29**, 2445-2455.
107. Y. Zhang, L. Charlet and P. W. Schindler, *Colloids Surf.*, 1992, **63**, 259-268.
108. B.-H. Jeon, B. A. Dempsey, W. D. Burgos and R. A. Royer, *Colloids Surf., A*, 2001, **191**, 41-55.



Iron mineral systems are effective at transforming highly oxidized contaminants in natural and engineered systems. The rate at which the contaminant degrades may be influenced by the amount of available mineral surface area. This study used dynamic light scattering and cryogenic transmission electron microscopy to monitor changes in the aggregation state of goethite nanoparticles before and after reaction with 4-chloronitrobenzene (4-CINB). The effects of buffer identity, buffer concentration, and adsorbing metal identity on the goethite nanoparticle suspension characteristics and reactivity were monitored. Results demonstrate that buffers, which serve to hold pH nearly constant over the course of a reaction, are not benign additives in batch reactors. In fact, the identity and concentration of the buffer used strongly influences the rate of 4-CINB degradation by surface-associated ferrous ion. Increasing buffer concentration resulted in more compact goethite nanoparticle aggregates, and slower 4-CINB degradation was observed. In addition, the rate of degradation changed dramatically with changing buffer identity, with rates of reaction changing by an order of magnitude when switching from 4-(2-hydroxyethyl)-1-piperazineethanesulfonic acid (HEPES) to Tris(2-hydroxyethyl)amine (TEA). Finally, of the three metal ions selected (Ca(II), Fe(II), and Co(II)), the addition and adsorption of the two transition metals resulted in a dramatic decrease in the average nanoparticle aggregate size. Furthermore, oxidation of the adsorbed Fe(II), via O_2 or 4-CINB reduction, yielded decreases in zeta potential and increases in aggregate size. This work demonstrates that small changes in reaction parameters have a large effect on the rate of contaminant degradation through changes in nanoparticle aggregation state.